Available online at www.sciencedirect.com

ScienceDirect

Procedia Structural Integrity 38 (2022) 611–620

Structural Integrity Procedia

www.elsevier.com/locate/procedia

FATIGUE DESIGN 2021, 9th Edition of the International Conference on Fatigue Design

Scatter and size effect in High Cycle Fatigue of cast aluminum-silicon alloys: A comprehensive experimental investigation

Driss EL KHOUKHI[1, 2, 3,*], Franck MOREL[1], Nicolas SAINTIER[2], Daniel BELLETT[1], Pierre OSMOND[3], Viet-Duc Le[1], Jérôme ADRIEN[4]

[1]*LAMPA, Arts et Métiers Paris Tech, 49 035 Angers, Cedex, France*
[2]*I2M, Arts et Métiers Paris Tech, 33170 Talence, Cedex, France*
[3]*STELLANTIS, 78955 Carrières-sous-Poissy, Cedex, France*
[4]*MATEIS, INSA de Lyon, 69621 Villeurbanne, Cedex, France*

Abstract

Cast Al-Si alloys have been widely used in automotive applications with regard to their low density and excellent thermal conductivity. Many components made of these alloys are subjected to cyclic loads which can lead to fatigue failure. For these materials, the well-known size effect in fatigue, whereby the fatigue strength is reduced when the size is increased, can be significant and needs to be properly evaluated. This paper analyses the role of casting defects on the fatigue scatter and size effect. A uniaxial fatigue testing campaign (R=0.1) has been conducted using two cast aluminum alloys, fabricated by different casting processes (gravity die casting and lost foam casting), associated with the T7 heat treatment, and with different degrees of porosity. The fatigue response of different specimens (smooth and notched) with different stressed volumes has been investigated. The first part of this article is about the experimental characterization of the size effect and scatter in both alloys via the concept of the Highly Stressed Volume. The second part investigates the effect of the Highly Stressed Volume on the critical defect size and the establishment of Kitagawa-Takahashi diagram. It is shown that the alloy B, with a population of defects of large size, shows a slight size effect and low scatter. In comparison, alloy A that exhibits a population of defects of relatively small size manifests significant size effect and high scatter.

Keywords: HCF ; size effect ; stress gradient effect ; Highly Stressed Volume ; microstructural heterogeneities ; cast aluminum alloys ; scatter.

1. Introduction

1.1 Context, introduction and objectives

The fatigue data transferability from laboratory specimens to real components or structures is very often difficult to handle because of the high number of parameters potentially affecting the fatigue strength. Besides the loading mode, the microstructural heterogeneities, the stress gradient, and the size of the loaded volume can show significant effects on the fatigue strength.

In particular, it is generally accepted that the fatigue strength of certain materials decreases with an increase in the volume (Kelly and Morrison 1970). This is referred to as either the “volume effect”, the “size effect” or the “scale effect” and is often simply explained by an increase in the probability of encountering a large material defect in the fatigue active volume.

* Corresponding author. Tel.: +33 (0) 6 48 50 81 78
E-mail address: driss.el-khoukhi@ensam.eu

10.1016/j.prostr.2022.03.063

Kloos in (Kloos et al. 1981) classified the size effect phenomenon into the following categories: (i) statistical size effect induced by the high probability of defects in larger specimens, (ii) geometrical size effect attributed to stress inhomogeneity from different notch types, this can also be referred to as the stress gradient effect, (iii) production size effect generated by production technology and (iv) surface size effect caused by the surface characteristics such as roughness.

Makkonen in (Makkonen 1999) proposed that the size effect, or the statistical size effect using Kloos' terminology, can be explained using the weakest link theory developed by (Weibull 1939). (Makkonen 1999) showed the influence of the statistical size effect on the high cycle fatigue behavior of both smooth and notched cylindrical specimens.

An example of fatigue design approach taking account of the size effect is the Highly Stressed Volume (HSV) approach which was first introduced by (Kuguel 1961). The terminology Vn% is used to define the volume of material that is subjected to at least n% of maximum principal stress ($\sigma n\% = n\% \times \sigma max$). This volume of material is assumed to have an increased probability of fatigue crack initiation. The percent is assumed to be 95% by (Kuguel 1961) and 90% by (Sonsino and Fischer 2005) and 80% by El Khoukhi in the present work and in previous publications (El Khoukhi et al. 2019; EL Khoukhi et al. 2018). Furthermore, the effect of HSV on the fatigue behavior has been well documented in references (Yang Ai et al. 2019; Zhu, Foletti, and Beretta 2018). It has been demonstrated that this approach yields accurate predictions for the fatigue behavior of both the notched and smooth specimens (Y. Ai et al. 2019).

This paper focuses on cast Al-Si alloys, widely used in the automotive industry. In order to manufacture engine components, Stellantis company indeed uses mainly two foundry processes that result in components containing Microstructural Heterogeneities (MH), principally shrinkage pores and oxides, with different characteristics (size, shape and spatial distributions). These components are subjected to cyclic mechanical loads (in the High Cycle Fatigue regime) that can result in the appearance of cracks and thus lead to the failure of the structure. The effect of the MH on the fatigue behavior has been well documented in references (Le et al. 2016; Koutiri et al. 2013; Osmond et al. 2018).

In the following study, two Al-Si alloys with different porosity distributions are chosen in order to understand how the characteristics of the defect populations affect the statistical size effect and scatter. Computed Tomography (CT) analyses are conducted in order to characterize the porosity in terms of size, shape and spatial distributions in these alloys. Different geometries (smooth and notched specimens) are used to work with different Highly Stressed Volumes. High cycle fatigue tests are conducted to investigate the size effect on the fatigue strength using the HSV concept. Fractographic analyses are also carried out to investigate the relationship between the critical defects and the fatigue strength via the Kitagawa-Takahashi diagram. The analyses of fatigue strength scatter are also conducted.

Even though this paper is about data already presented in reference (El Khoukhi et al. 2019), it is worth mentioning that new results and original analyses are proposed. In particular, test results on smooth specimens and notched samples designed to prevent local plasticity are added to the large database. An original investigation on the fatigue scatter is also proposed and helps getting a better knowledge of the role played by the defect population on the fatigue strength distribution.

2. Materials and experimental conditions

2.1 Mechanical and Material Properties

To study the influence of casting defects on the statistical size effect, two primary cast aluminum alloys, referred to as alloys A [AlSi7Cu05Mg03-T7] and B [AlSi7Mg03-T7], have been used (see Figure 1). These alloys were fabricated by different casting processes (alloy A: gravity die-casting and Alloy B: lost foam casting), and subject to the T7 heat treatment. These processes result in different porosity populations (i.e. volume fraction, defect size…) and different mechanical properties (table 1). Previous works concerning the characterization of these materials have been done by (Le et al. 2016) and (Koutiri et al. 2013). Table 1 summarizes the material properties of these alloys (Le et al. 2016 ; Koutiri et al. 2013).

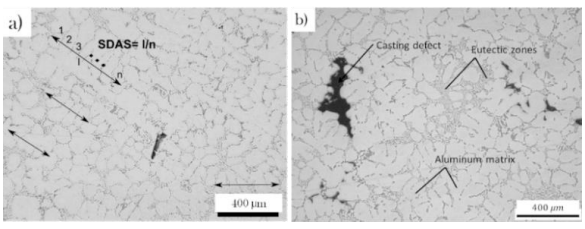

Figure 1: The microstructure of the investigated alloys (a) Alloy A (AlSi7Cu05Mg03 - T7) (b) Alloy B (AlSi7Mg03 - T7).

Table 1 : Properties of the investigated cast Al-Si alloys

Grade	Alloy A	Alloy B
Designation	AlSi7Cu05Mg03 - T7	AlSi7Mg03 - T7
Casting Process	Gravity Die	Lost Foam
Heat treatment	T7	T7
SDAS (µm)	42±10	77±19
Young Modulus E (GPa)	77±6 [16]	68±5 [16]
Yield stress $\sigma_{Y0.2\%}$ (MPa)	260±2	240±5
Ultimate tensile strength σ_u (MPa)	304±4	251±6
Elongation A (%)	4.7±1.2	0.8±0.1
Porosity (%)	0.03	0.28
Micro-hardness (Hv25Gr)	115	100

From Table 1, we can notice a difference in terms of micro-hardness, yield stress, ultimate strength and Young modulus, SDAS parameter related to the grain size and elongation between the studied materials. However, it is well known that the uniaxial fatigue resistance in the HCF regime is mainly controlled by the defect size (Koutiri et al. 2013; Ben Ahmed et al. 2017).

2.2 Defect population characterization

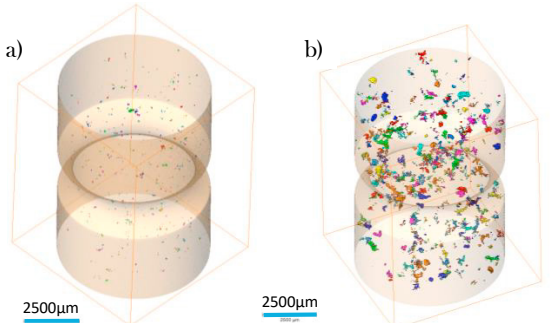

Figure 2: Micro-tomography scans of the alloys (a) alloy A and (b) alloy B.

In order to characterize the defect size distribution in these alloys, (CT) analyses were undertaken. CT scans were done by the MATEIS laboratory at INSA Lyon with resolution of 8 µm/voxel. The AVIZO® software was then used in order to analyze the raw data. The alloys were characterized in terms of size and shape distributions of their porosity. An inspection volume of 363 mm^3 was used. Figure 2 illustrates the defect population as imaged by microtomography on two notched fatigue specimens. It can be clearly seen that alloy B has considerably larger pores when compared to alloy A.

Figure 3 -a- shows the defect size distributions for the two alloys in terms of the equivalent Murakami parameter (Murakami 1991), $\sqrt{Area}_{eq}$ of the defect. The relationship between pore volume obtained by tomography and its equivalent square root of the projected area is given in (eq. 1). This relationship is obtained by assuming a spherical pore shape.

$$\sqrt{Area}_{eq} = \pi^{1/6} \left(\frac{3V}{4}\right)^{1/3} \quad \text{(eq. 1)}$$

In the investigated volume, the maximum pore sizes in terms of the $\sqrt{Area}_{eq}$ parameter, obtained in the scanned volumes, are 166 µm for alloy A and 302 µm for alloy B. Almost all the defects in alloy A have a $\sqrt{Area}_{eq}$ lower than 100 µm whereas 20% of the defects in alloy B have a $\sqrt{Area}_{eq}$ greater than 100 µm. In order to characterize the shape of the defects, the sphericity parameter is defined in equation (eq. 2).

$$S = \frac{\pi^{1/3}(6V)^{2/3}}{A} \quad \text{(eq. 2)}$$

where A is the surface area of the pore and V is the pore volume. This parameter compares the shape of a pore to a sphere, only the perfect sphere will have a sphericity of 1. Figure 3 -b- shows the relationship between pore size and sphericity for both alloys. It can be seen that the largest pores have the lowest sphericity and a complex shape. This tendency has also been observed in

previous works (Le et al. 2016; Buffière et al. 2001). This repartition tends to indicate the presence of shrinkage porosity and gas pores. This last type of pores seems especially present in the alloy B.

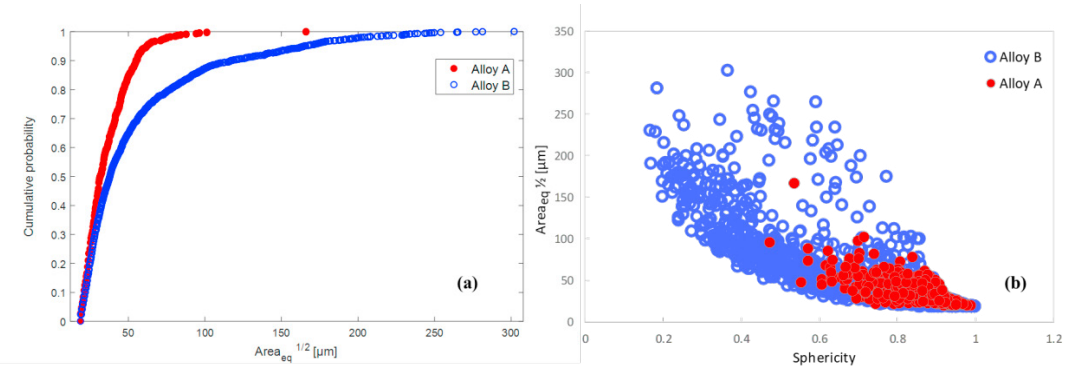

Figure 3: (a) Distributions of the defect size of the pores from the scanned specimens in Fig. 2. (b) Defect size as a function of the sphericity of the defects.

The alloys have different characteristics in terms of size and shape. We can summarize the data as follows:

- Alloy B contains larger pores than alloy A.
- Alloy A presents more regular shaped pores compared to alloy B.

For the record, a complete description of the spatial distribution of the defects is presented in (El Khoukhi, et al. 2021).

3. Experimental conditions of the fatigue tests

All fatigue tests were performed under uniaxial tensile loads with a stress ratio R = 0.1 using a Rumul Testronic resonant testing machine at approximately 105 Hz. The stopping criterion was a drop in the resonance frequency of 1 Hz, corresponding to the presence of a fatigue crack of approximately 2 mm on surface. All tests were performed at room temperature, in air. The tests were conducted following the staircase method with a maximum life of 2 million cycles. The run-out specimens were retested until failure at higher load levels in order to identify the critical defect that initiates a crack. A step of 5 MPa stress amplitude was used in the staircase procedure. The data of fatigue strength were also analyzed using the Lanning (Lanning et al. 2005) formula in order to estimate the fatigue strength of every single sample.

3.1 Specimen geometry

To study the effect of stressed volume on the fatigue strength of alloys A and B, different fatigue specimen geometries were defined, corresponding to different loaded volumes. These are shown in Figure 4 and are referred to as: “V1-Small Volume”, “V2-Reference Volume”, “V3-Large Volume” and “VN-Notched specimen with Kt of 1.68”. We remined that the Ra surface finish after machining of the samples was with a value Ra of 0.8.

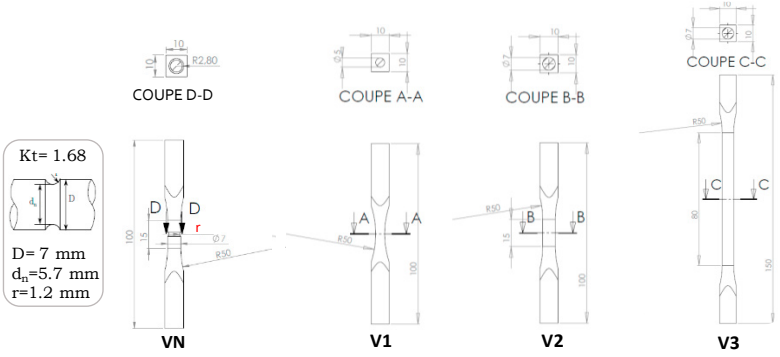

Figure 4: Specimens for tensile fatigue tests

3.2 Estimation of the Fatigue Active Volume

To illustrate the difference between the four specimen geometries in terms of loaded volume, the concept of the Fatigue Active Volume "FAV" is used in an empirical manner. In the following sections, the FAV is estimated using the combination of two criteria:

Damage mechanism: In the literature, much works (Le et al. 2016; Boromei et al. 2010) have shown that the fatigue failure usually occurs at defect or pores located on the surface or in a sub-surface layer. In the experimental work undertaken in this work, the crack initiation sites are located in a subsurface of 500 µm for alloy A and 650 µm for alloy B. Figure 5-a- shows a subsurface pore with the depth 't' in the crack initiation zone for alloy B. Figure 5-b- shows the cumulative distributions distance from the surface for all pores observed in the crack initiation zones in these alloys.

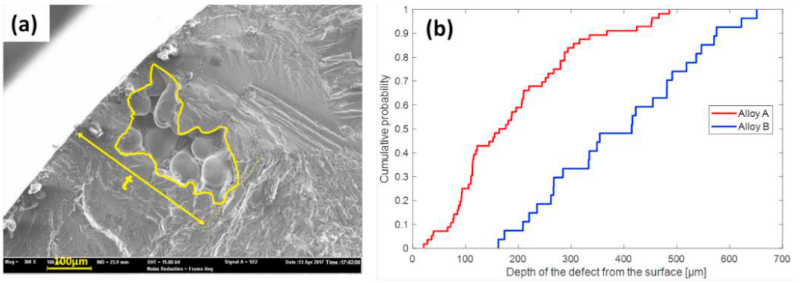

Figure 5: (a) The definition of the depth of a critical defect, and (b) Cumulative probability of the defect depths for the alloys

Stress heterogeneity: A Highly Stressed Volume of V80% is chosen. The justification for choosing this value is based on the results for the V1 specimen, which has an hourglass shape (Figure 6). Most of the fatigue cracks in these specimens do not occur in the center of the specimen where the cross-sectional area is the smallest and the stress is the highest. This is because the cast aluminum materials investigated are defect containing materials. Figure 6 -a - shows the case of a specimen in which the fatigue crack is located approximately 5.82 mm from the middle of the specimen. Figure 6 -b- shows the normalized stress at the crack location as a function of the distance from the center of the specimen. From this figure, it can be seen that almost all of the specimens have failed at a stress level that is greater than 80% of the maximal stress.

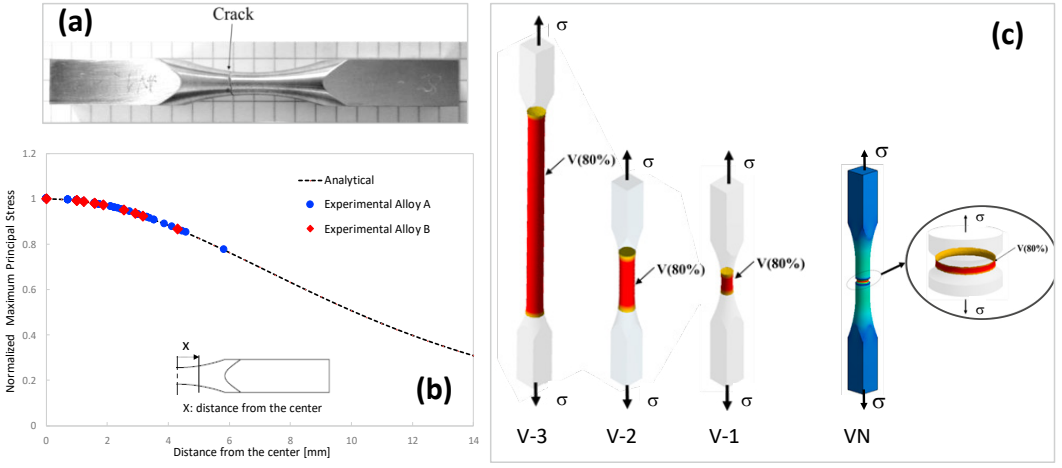

Figure 6: (a) AV1 specimen showing that the fatigue crack is not necessarily located in the center of the specimen. (b) Fatigue crack localization in the hour-glass shaped V1 specimens. (c) Highly Stressed Volume for (a) smooth specimens V1, V2 and V3 and (b) notched specimen.

The combination of these two criteria is used to define the Highly Stressed Volume corresponding to $0.8\sigma_{Imax}$ located in a subsurface layer of thickness 500 µm for alloy A and 650 µm for alloy B. In the following section, this definition is referred to as the FAV. For each specimen geometry, an estimation of the Highly Stressed Volume has been done using finite element computation with a linear elastic analysis. Figure 6 -c- shows HSVs identified for each case.

The use of the notch for the fatigue specimens AVN and BVN has been designed to get a very small active volume.

In the following sections, we will use the estimated FAV_A for alloy A and FAV_B for alloy B. The FAV corresponding to each specimen shape, as well as stress concentration factors and number of specimens tested for each configuration, are presented in Table 2. We point out also that the FAV of the sample V3 for alloy B is not indicated in Table 2 since it was not tested for this alloy. The stress concentration factors Kt were estimated as follows in (eq. 3):

$$K_t = \frac{\sigma_{max}}{\sigma_{nom}} \quad \text{(eq. 3)}$$

Where, σ_{max} being the maximum elastic normal stress in the axial direction at the notch tip, and σ_{nom} is the nominal elastic stress based on the net section.

Table 2 : Characteristics of the samples

Sample	Number of specimens		Kt	FAVA in mm3 for the sublayer of 500 µm	FAVB in mm3 for the sublayer of 650 µm	Stress Gradient X [mm-1]
	Alloy A	Alloy B				
VN	50	23	1.68	5	6	1
V1	47	12	1	90	110	Close to 0
V2	46	12	1	320	450	0
V3	12	0	1	912	-	0

4. Fatigue SN curves and statistical size effect

4.1 High cycle Fatigue S-N Curves

Figure 7 shows the S-N curves for the different batches. It can be seen that the fatigue resistance for the different batches of the alloy A is higher than the fatigue resistance for the batches of alloy B. Therefore, the fatigue resistance of cast aluminum alloys is strongly linked to the defect population of these alloys.

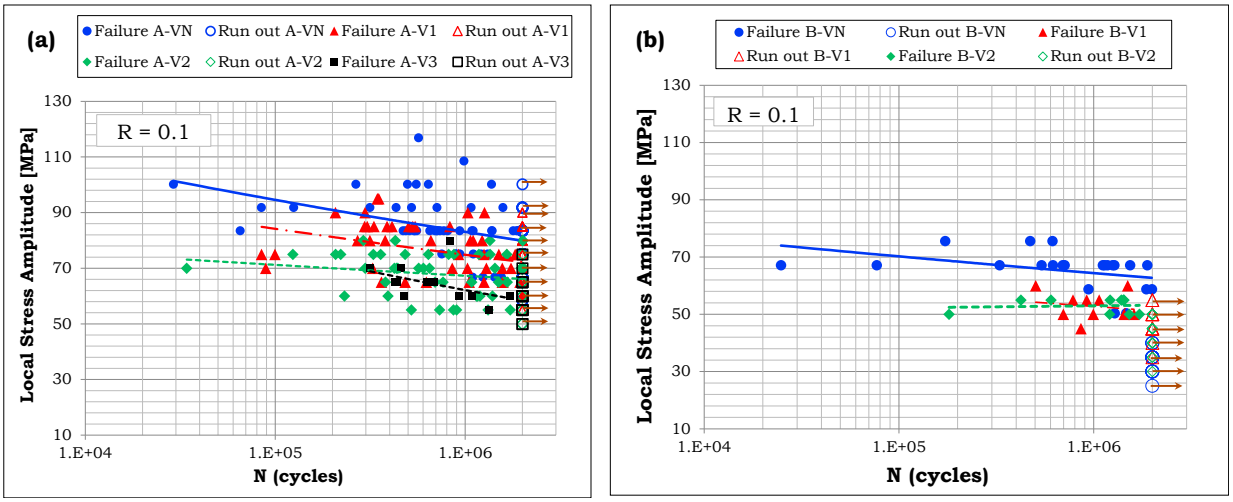

Figure 7: SN-Curves plotted in semi-Linear diagram (a) for the alloy A and (b) for the alloy B.

4.2 Crack initiation Mechanisms

After fatigue failure, the crack initiation sites were systematically observed on all specimens. Different defect types were identified to be at the origin of fatigue crack initiation and are discussed below. SEM was used to measure Murakami parameter $\sqrt{\text{Area}}$ of the critical defects on the fatigue failure surfaces.

- Figure 8 -a- highlights the importance in fatigue of the free surface. For this specimen, a very large defect can be seen in the middle of the specimen ($\sqrt{Area}$ = 575 µm) and a smaller one is visible near the surface ($\sqrt{Area}$ = 367 µm). The SEM observations clearly show that the smaller pore close to the surface is responsible for the fatigue failure.
- For alloy B, all the crack initiation sites are pores. In contrast, for alloy A, which has a lower density of large pores, other crack initiation mechanisms were observed such as initiation from oxides and Persistent Slip Band (Figure 10 -b- and -d-). However, the dominant fatigue damage mechanism is crack initiation and growth from pores (Figure 10 -c-).

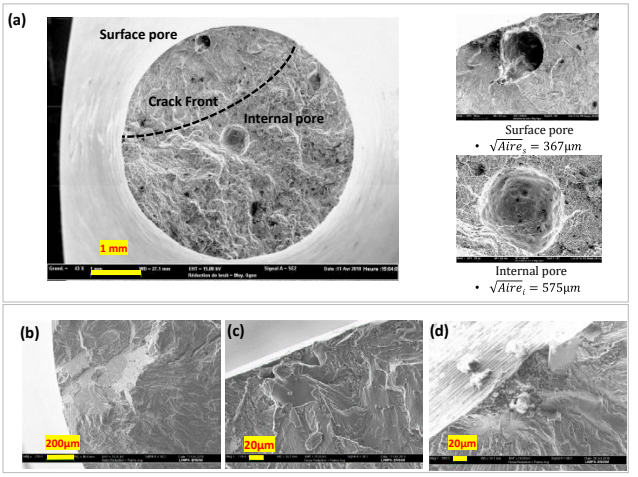

Figure 8: (a) Fatigue failure, specimen BV1-05, Sa= 55 MPa, Nf=919402 cycles, this sample presents a surface and internal pore.(b) specimen AV1-44, Sa= 85 MPa, Nf= 545162 cycles, crack initiation from persistent slip band (PSB), (c) specimen AV1-43, Sa= 65 MPa, Nf= 1581225 cycles, crack initiation from pore at the surface. And (d) specimen AVN-04, Sa= 50 MPa, Nf= 1084107 cycles, crack initiation from an oxide at the surface.

4.3 Effect of the Fatigue Active Volume on the critical defect size

Figure 9 shows the evolution of the critical defect sizes as a function of the Fatigue Active Volume for both alloys.

- The mean value of critical defect size in alloy B is larger than 225 µm, and for alloy A, the mean value of critical defect size is less than 210 µm.
- The curves show the same tendencies. For a small FAV, the average critical defect size is low. It starts to increase and then stabilizes for a FAV of approximately 110 mm^3 for alloy B and a FAV of 320 mm^3 for alloy A.
- For alloy A, that shows different types of mechanisms of failure (pores, oxides and PSBs), the average size of critical defects estimated from pores (red points in figure 11), and the average size of critical defects estimated for 'pores + oxides' (see green cross in the figure 11), it seems that they have almost the same average size.

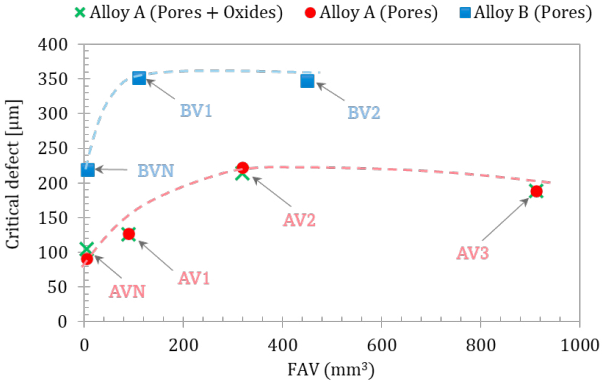

Figure 9: The critical defect size as a function of the Fatigue Active Volume

4.4 Role of defect size population on Statistical size effect and fatigue strength scatter

In order to illustrate the influence of the size effect on the fatigue strength, the product of the nominal stress amplitude Σ_D and stress concentration factor Kt is used. That is, for the notched specimens the local stress amplitude at the notch-tip is used. In references (Engelke and Esderts 2018 ; Lipp et al. 2013), it was shown that there is a good correlation between the fatigue strength expressed as $K_t\Sigma_D$ and the highly stressed volume. In this work, the correlation will be made in terms of the FAV. Let

us also notice that the estimation of the fatigue limit of each specimen is assessed using the following formula (eq. 4) proposed in (Lanning et al. 2005).

$$\Sigma_D = \sigma_{n-1} + (\sigma_n - \sigma_{n-1}) \times \frac{N_f}{2\times10^6} \quad \text{(eq. 4)}$$

where Σ_D is the interpolated fatigue limit at 2 millions of cycles. σ_{n-1} is the stress amplitude level of the block prior to the block where failure occurs. For the specimens that fail at the first level (σ_n) of stress, we supposed the existence of a fictive level (σ_{n-1}). σ_n is the maximum stress level of the final block of cycles during which failure occurs, and Nf is the number of cycles to failure in the final loading block. The main objective here is to get the fatigue limit of each specimen and not for the whole batch. The results are presented in Figure 10.

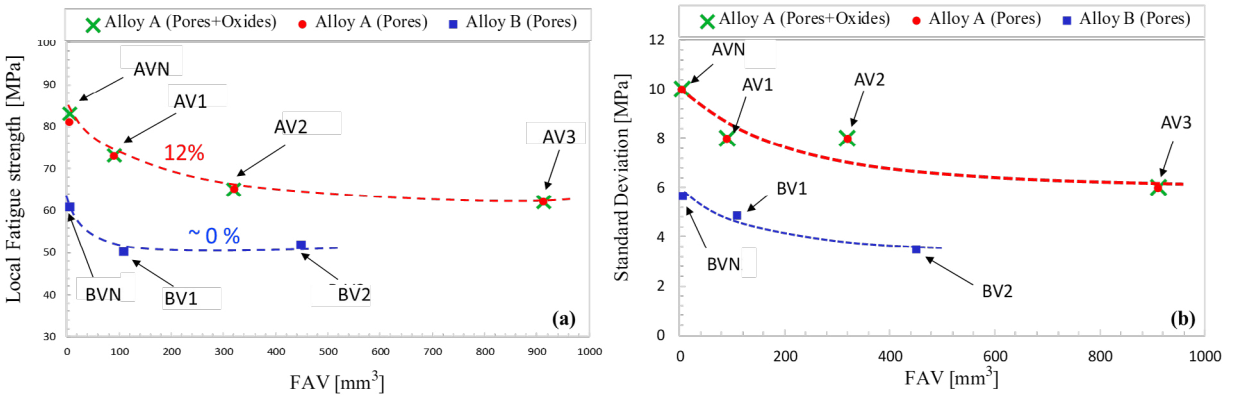

Figure 10: (a) local fatigue resistance and (b) its standard deviation as function of FAV for alloys A and B.

Figure 10 -a- shows the effect of the fatigue active volume (FAV) on the local fatigue strength amplitude $K_t\Sigma_D$ for 50% probability of failure for a stress ratio of R = 0.1 at 2×10^6 cycles.

- For both alloys, the local fatigue strength amplitude decreases with increasing FAV, then stabilizes for each alloy at a specific FAV. The notched specimens show the highest strengths in terms of the local stress amplitude.
- The alloy A has a more pronounced volume effect than alloy B. Indeed, a drop of 20 MPa approximately in local fatigue limit from AVN to AV3. In contrast, the drop for the alloy B is almost 10 MPa from BVN to BV2.
- The presence of oxides as mechanisms of failure does not induce big difference in the resulted behavior of fatigue strength. This result is consistent with the literature (Rotella 2017).
- For alloy A, the fatigue strength stabilizes from a specific volume of roughly 320 mm^3. While for alloy B, the fatigue strength stabilizes rapidly at volume of roughly 110 mm^3. These volumes could be considered as the Representative Element Volumes (REV).

Figure 10 -b- presents the evolution of the standard deviation of the studied alloys with the size of fatigue active volume.

- Both alloys show the same tendency in standard deviation of fatigue strength. The standard deviation in fatigue strength is high for the smaller volumes and decreases by increasing the volume of the sample.
- The results show that the alloy A with small defect sizes shows a high scatter compared to the alloy B with larger defects.
- For the alloy A, taking in account the data associated to both mechanisms, oxide and pore or only pores lead to the same value of scatter.

5. Kitagawa-Takahashi diagram

In order to link the fatigue strength of the different specimens to the critical defect size, Kitagawa-Takahashi diagrams have been built. The estimation of fatigue strength for each specimen was carried out using the local stress. Results are shown in Figure 11. It shows the linear representation of Kitagawa-Takahashi diagram in terms of local fatigue limit $K_t\Sigma_D$ as a function of the average of the square root of the critical defect size of each batch.

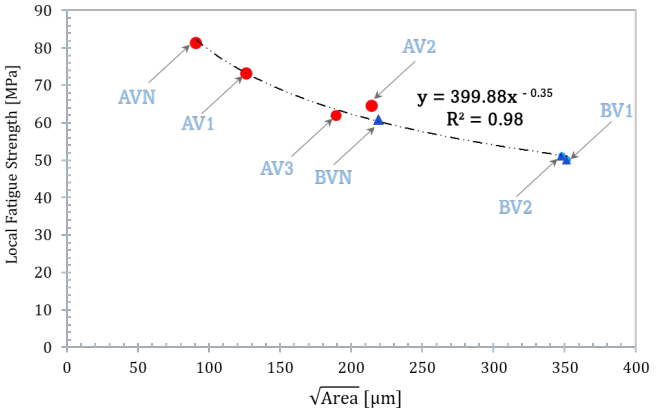

Figure 11: local fatigue resistance as a function of critical defect size (R=0.1), known as Kitagawa-Takahashi diagram.

From Figure 11 the following conclusions can be made:

- The fatigue strength of the alloys tends to decrease when the size of the critical defects increases then stabilizes.
- For the alloy A, most of the critical defects are situated in the interval with high slope in the diagram.
- For the smooth samples of the alloy B (BV1 and BV2), the critical defect sizes lie in the range where the fatigue strength begins to stabilize.

6. Synthesis and discussion

Figure 12 is a schematic representation of the fatigue strength amplitude as a function of the critical defect size for volumes AV1, AV2, BV1 and BV2. It shows that for the alloy A, a difference in the average size of the critical defects between the batches AV1 and AV2 leads to a significant difference in the fatigue strength of these batches. For that reason, the size effect and the fatigue strength scatter are high for the alloy A.

In contrast, the average of critical defect sizes of the batches BV1 and BV2 lie in the range where the curve shows a slight slope. Therefore, for alloy B, even if there is a noticeable difference in the average size of critical defects between the batches BV1 and BV2, however the difference between the fatigue strength of these two batches is very small. Therefore, a non-significant size effect and low scatter are resulted.

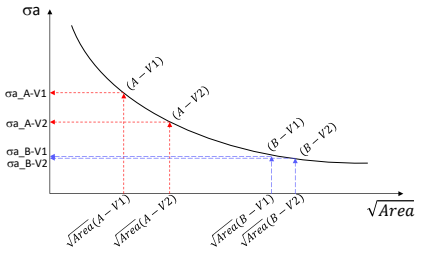

Figure 12: Schematic representation of fatigue resistance as a function of average size of the critical defects for each batch.

7. Conclusions

In this study, an experimental investigation has been conducted to evaluate the statistical size effect on the fatigue strength of cast Al-Si alloys. The main results can be summarized as follows:

- The fatigue strength and its scatter are strongly dependent on microstructure defects in cast aluminum alloys. The most harmful defects are the pores located on specimen surface or subsurface, and the pore size is the key factor controlling fatigue strength and its scatter. These results have been confirmed using a probabilistic model by (El Khoukhi, et al. 2021).
- A variation in the highly stressed volume leads a change in the fatigue strength of the material. This result confirms the existence of a size effect in cast Al-Si alloys. Furthermore, alloy A has a more pronounced volume effect than alloy B.

- The fatigue strength for alloy A stabilizes from a critical volume of roughly 320 mm^3, which can be considered as the Fatigue Representative Elementary Volume. While the fatigue strength of alloy B stabilizes at a smaller critical volume of 110 mm^3 which can be considered as the fatigue RVE of this alloy.
- In terms of fatigue damage mechanisms, for the alloy B, all the specimens have shown fracture initiated from a pore. However, the alloy A shows several mechanisms of crack initiation (pores, oxide, PSB).
- Size effect and scatter of fatigue are strongly linked to the defect size distribution. Small size defect distribution (Alloy A) leads to high scatter and high size effect in fatigue strength.

Acknowledgments

The authors gratefully acknowledge the financial support of the OPENLAB Materials and Processes, and the French National Agency for Research and Technology (ANRT).

References

Ai, Y., S. P. Zhu, D. Liao, J. A. F. O. Correia, C. Souto, A. M. P. De Jesus, and B. Keshtegar. 2019. "Probabilistic Modeling of Fatigue Life Distribution and Size Effect of Components with Random Defects." *International Journal of Fatigue* 126 (September): 165–73. https://doi.org/10.1016/j.ijfatigue.2019.05.005.

Ai, Yang, Shun-Peng Zhu, Ding Liao, José A. F. O. Correia, Abílio M. P. De Jesus, and Behrooz Keshtegar. 2019. "Probabilistic Modelling of Notch Fatigue and Size Effect of Components Using Highly Stressed Volume Approach." *International Journal of Fatigue* 127 (October): 110–19. https://doi.org/10.1016/j.ijfatigue.2019.06.002.

Ben Ahmed, A., A. Nasr, A. Bahloul, and R. Fathallah. 2017. "The Impact of Defect Morphology, Defect Size, and SDAS on the HCF Response of A356-T6 Alloy." *The International Journal of Advanced Manufacturing Technology* 92 (1): 1113–25. https://doi.org/10.1007/s00170-017-0192-6.

Boromei, I, L Ceschini, Al Morri, An Morri, G Nicoletto, and E Riva. 2010. "Influence of the Solidification Microstructure and Porosity on the Fatigue Strength of Al-Si-Mg Casting Alloys" 28: 7.

Buffière, J-Y., S. Savelli, P. H. Jouneau, E. Maire, and R. Fougères. 2001. "Experimental Study of Porosity and Its Relation to Fatigue Mechanisms of Model Al–Si7–Mg0.3 Cast Al Alloys." *Materials Science and Engineering: A* 316 (1): 115–26. https://doi.org/10.1016/S0921-5093(01)01225-4.

EL Khoukhi, Driss, Franck Morel, Nicolas Saintier, Daniel Bellett, and Pierre Osmond. 2018. "The Effect of Microstructural Heterogeneities on the High Cycle Fatigue Scatter of Cast Aluminium Alloys: From an Elementary Volume to the Structure." *MATEC Web of Conferences* 165: 14006. https://doi.org/10.1051/matecconf/201816514006.

El Khoukhi, Driss, Franck Morel, Nicolas Saintier, Daniel Bellett, Pierre Osmond, and Viet-Duc Le. 2021. "Probabilistic Modeling of the Size Effect and Scatter in High Cycle Fatigue Using a Monte-Carlo Approach: Role of the Defect Population in Cast Aluminum Alloys." *International Journal of Fatigue* 147 (June): 106177. https://doi.org/10.1016/j.ijfatigue.2021.106177.

El Khoukhi, Driss, Franck Morel, Nicolas Saintier, Daniel Bellett, Pierre Osmond, Viet-Duc Le, and Jérôme Adrien. 2019. "Experimental Investigation of the Size Effect in High Cycle Fatigue: Role of the Defect Population in Cast Aluminium Alloys." *International Journal of Fatigue* 129 (December): 105222. https://doi.org/10.1016/j.ijfatigue.2019.105222.

El Khoukhi, Driss, Nicolas Saintier, Franck Morel, Daniel Bellett, Pierre Osmond, and Viet-Duc Le. 2021. "Spatial Point Pattern Methodology for the Study of Pores 3D Patterning in Two Casting Aluminium Alloys." *Materials Characterization* 177 (July): 111165. https://doi.org/10.1016/j.matchar.2021.111165.

Engelke, Torben, and Alfons Esderts. 2018. "Analytical Strength Assessments of Austempered Ductile Iron Components," 5.

Kelly, D. A., and J. L. M. Morrison. 1970. "Effect of Specimen Size and Preparation on the Fatigue Strength of a Plain Carbon Steel Tested in Rotating Bending and in Torsion." *Proceedings of the Institution of Mechanical Engineers* 185 (1): 655–64.

Kloos, K. H., A. Buch, and D. Zankov. 1981. "Pure Geometrical Size Effect in Fatigue Tests with Constant Stress Amplitude and in Programme Tests." *Materialwissenschaft Und Werkstofftechnik* 12 (2): 40–50. https://doi.org/10.1002/mawe.19810120205.

Koutiri, Imade, Daniel Bellett, Franck Morel, Louis Augustins, and Jérôme Adrien. 2013. "High Cycle Fatigue Damage Mechanisms in Cast Aluminium Subject to Complex Loads." *International Journal of Fatigue* 47 (February): 44–57. https://doi.org/10.1016/j.ijfatigue.2012.07.008.

Kuguel, R. 1961. "A Relation between Theoretical Stress Concentration Factor and Fatigue Notch Factor Deduced from the Concept of Highly Stressed Volume." *ASTM Proc.* 61: 732–48.

Lanning, David B., Theodore Nicholas, and George K. Haritos. 2005. "On the Use of Critical Distance Theories for the Prediction of the High Cycle Fatigue Limit Stress in Notched Ti–6Al–4V." *International Journal of Fatigue* 27 (1): 45–57. https://doi.org/10.1016/j.ijfatigue.2004.06.002.

Le, Viet-Duc, Franck Morel, Daniel Bellett, Nicolas Saintier, and Pierre Osmond. 2016. "Multiaxial High Cycle Fatigue Damage Mechanisms Associated with the Different Microstructural Heterogeneities of Cast Aluminium Alloys." *Materials Science and Engineering: A* 649 (January): 426–40. https://doi.org/10.1016/j.msea.2015.10.026.

Lipp, K., J. Baumgartner, and P. Beiss. 2013. "Fatigue Design of Sintered Steel Components: Effect of Stress Concentrations and Mean Stresses on Local Strength Using Highest Stressed Volume Approach." *Powder Metallurgy* 56 (5): 337–41. https://doi.org/10.1179/0032589913Z.000000000141.

Makkonen, Matti. 1999. "Size Effect and Notch Size Effect in Metal Fatigue," August. http://lutpub.lut.fi/handle/10024/46785.

Murakami, Yukitaka. 1991. "Effects of Small Defects and Nonmetallic Inclusions on the Fatigue Strength of Metals." Key Engineering Materials. Trans Tech Publications Ltd. 1991. https://doi.org/10.4028/www.scientific.net/KEM.51-52.37.

Osmond, Pierre, Viet-Duc Le, Franck Morel, Daniel Bellett, and Nicolas Saintier. 2018. "Effect of Porosity on the Fatigue Strength of Cast Aluminium Alloys: From the Specimen to the Structure." *Procedia Engineering*, 7th International Conference on Fatigue Design, Fatigue Design 2017, 29-30 November 2017, Senlis, France, 213 (January): 630–43. https://doi.org/10.1016/j.proeng.2018.02.059.

Rotella, Antonio. 2017. "Fatigue d'un alliage d'aluminium moulé A357-T6 : rôle de la morphologie, de la position des défauts et application à une structure pour le calcul de la durée de vie en fatigue," October. https://tel.archives-ouvertes.fr/tel-01692427.

Rotella, Antonio, Yves Nadot, Mickaël Piellard, Rémi Augustin, and Michel Fleuriot. 2020. "Influence of Defect Morphology and Position on the Fatigue Limit of Cast Al Alloy: 3D Characterization by X-Ray Microtomography of Natural and Artificial Defects." *Materials Science and Engineering: A* 785 (May): 139347. https://doi.org/10.1016/j.msea.2020.139347.

Sonsino, C. M., and G. Fischer. 2005. "Local Assessment Concepts for the Structural Durability of Complex Loaded Components." *Materialwissenschaft Und Werkstofftechnik* 36 (11): 632–41.

Weibull, Waloddi. 1939. *The Phenomenon of Rupture in Solids,*. Stockholm: Generalstabens litografiska anstalts förlag.

Zhu, Shun-Peng, Stefano Foletti, and Stefano Beretta. 2018. "Evaluation of Size Effect on Strain-Controlled Fatigue Behavior of a Quench and Tempered Rotor Steel: Experimental and Numerical Study." *Materials Science and Engineering: A* 735 (September): 423–35. https://doi.org/10.1016/j.msea.2018.08.073.